Supporting Information

Carbon Support Tuned Electrocatalytic Activity of Single-Site Metal-organic Framework toward Oxygen Reduction Reaction

Wenjie Ma,[a] Fei Wu,[a] Ping Yu[ac] and Lanqun Mao*[ab]

[a] Beijing National Laboratory for Molecular Sciences, Key Laboratory of Analytical Chemistry for Living Biosystems, Institute of Chemistry, The Chinese Academy of Sciences (CAS), Beijing 100190, China

[b] College of Chemistry, Beijing Normal University, Xinjiekouwai Street 19, Beijing 100875, China

[c] University of Chinese Academy of Sciences, Beijing 100049, China

* Email: lqmao@iccas.ac.cn

Table of Contents

S1- Experimental Section

1 Chemical Reagent

Graphene oxide (GO) was bought from Carmery Materials Technology. Multi-walled carbon nanotube (CNT) was bought from XFNANO. $Al_2(SO_4)_3 \cdot 18H_2O$, $AlCl_3 \cdot 6H_2O$, formic acid, ammonium formate, urea, concentrated HNO_3, concentrated H_2SO_4, $CoCl_2 \cdot 6H_2O$, DMF and DMSO were purchased from Beijing Chemical Reagents. Meso-tetra(4-carboxylphenyl) porphyrin (TCPP) was obtained from Frontier Scientific. All these chemicals were used without any further purification. Aqueous solutions were all prepared with pure water obtained from a Milli-Q water system (Millipore, 18.2 MΩ cm). Unless stated otherwise, all experiments were carried out at room temperature.

2 Experimental Details

2.1 Materials Synthesis

Preparation of cobalt meso-tetra(4-carboxylphenyl) porphyrin (Co-TCPP)

Co-TCPP was synthesized with slight modification according to the previous literature.[1] Typically, 142 mg TCPP and 100 mg $CoCl_2 \cdot 6H_2O$ were dissolved in 60 mL DMSO and the mixture was heated to reflux for 24 h under N_2 atmosphere. After the solution was cooled to room temperature, 120 mL of 1 M HCl was added to precipitated porphyrin. The precipitates was obtained by centrifugation and washed with diluted HCl and H_2O for several times. The obtained solid was dissolved in 40 mL of 0.1 M NaOH, and the solution was filtrated to remove insoluble impurities. The filtrate was acidified with 1 M HCl to precipitate the metalated porphyrin. Co-TCPP was obtained by washing the precipitates with H_2O for several times and drying.

Preparation of Co-MOF

Co-MOF was synthesized via microwave-assisted solvothermal synthesis.[1] Typically, 14 mg Co-TCPP and 30 mg $AlCl_3 \cdot 6H_2O$ were dissolved in 3 mL H_2O in a microwave tube. The tube was sealed, sonicated for 20 min and put in a microwave reactor (NOVA-2S, PreeKem Scientific Instruments). The mixture was rapidly heated to 160 °C within 3 min and kept at 160 °C for 1 h. After cooling to room temperature, the solid was collected by centrifugation, washed with DMF and water for several times and finally dried at 80 °C under vacuum for 12 h. The dark-red product of Co-MOF was obtained.

Preparation of Co-MOF@CNT

The synthesis of Co-MOF@CNT includes the deposition of aluminum hydroxide onto the surface of CNTs to form CNT-Al and the transformation of CNT-Al into Co-MOF@CNT under microwave heating. CNT-Al was fabricated with slight modification following a reported method.[2] In a typical synthesis, 5 mg oxidized CNTs (ox-CNTs) prepared by sonicating CNTs in the mixture of H_2SO_4 and HNO_3 (3:1) was dispersed in 5 mL of 0.2 M formic acid-ammonium formic buffer solution (pH=4.4) under sonication, and then different amounts of $Al_2(SO_4)_3 \cdot 18H_2O$ (5 mg, 15 mg and 45 mg) were added. The mixture was heated at 70 °C for 2 h with continuous stirring. After cooling to room temperature, the solid was isolated by centrifugation and washed with water for serval times and dried at 80 °C for

24 h under vacuum. For the transformation of CNT-Al into Co-MOF@CNT, 2 mg CNT-Al and 4 mg Co-TCPP were dispersed in the mixed solvent of 1 mL DMF and 1 mL H_2O, and then the mixture was transferred into a microwave tube and heated at 140 °C for 1 h in a microwave reactor. After cooling to room temperature, the solids were collected by centrifugation and washed with DMF and water for several times and finally lyophilized to obtain Co-MOF@CNT-**1**, Co-MOF@CNT-**2** and Co-MOF@CNT-**3**.

Preparation of Co-MOF@rGO

Similarly, the synthesis of Co-MOF@rGO includes the deposition of aluminum hydroxide onto the surface of GO to form GO-Al and the transformation of GO-Al into Co-MOF@rGO under microwave heating. GO-Al was synthesized according to the previous study.[3] Typically, 18 mg urea was dissolved in 10 mL solution of 5 mM $Al_2(SO_4)_3$, and the solution was added into 10 mL of GO aqueous dispersion (2 mg/mL). Then, the mixture was heated at 95 °C for 3 h under continuous stirring. When the mixture cooled down to room temperature, the brownish black precipitation was collected by centrifugation, washed with pure water for several times and finally lyophilized to obtain GO-Al-1. GO-Al-2, GO-AL-3 and GO-AL-4 were synthesized by the same method with the use of 72 mg urea and 20 mM $Al_2(SO_4)_3$, 360 mg urea and 100 mM $Al_2(SO_4)_3$, 1800 mg urea and 500 mM $Al_2(SO_4)_3$, respectively. For the transformation of GO-Al into Co-MOF@rGO, 2 mg GO-Al and 4 mg Co-TCPP were dispersed in the mixed solvent of 1 mL DMF and 1 mL H_2O, and then the mixture was transferred into a microwave tube and heated at 140 °C for 1 h in a microwave reactor. After cooling to room temperature, the solids were collected by centrifugation and washed with DMF and water for several times and finally lyophilized to obtain Co-MOF@rGO-**1**, Co-MOF@rGO-**2**, Co-MOF@rGO-**3** and Co-MOF@rGO-**4**.

2.2 Instrument and Characterization

SEM images were taken with field-emission scanning electron microscopes (Hitachi-SU8020). TEM images were obtained by using a F JEOL JEM-2011F high-resolution transmission electron microscope operated at 200 kV. The energy dispersion spectroscopy analysis was carried out on an energy dispersive spectrometer (ZNCA Energy TEM 100 X-ray energy spectrum) assembled on the JEM-2100F. Powder X-ray diffraction (PXRD) patterns were performed on a Rigaku RU-200b X-ray powder diffractometer with Cu Kα radiation (λ = 1.5406 Å). X-Ray photoelectron spectra (XPS) were collected on VG Scientific ESCALab220i-XL X-Ray photoelectron spectrometer, using Al Ka radiation as the excitation sources. Binding energies obtained in the XPS analysis were corrected with reference to C1s (284.8eV). Raman spectra were recorded on a LabRAM ARAMIS Raman spectrometer at resolution of 2 cm^{-1} by using the 532 nm line of an Argon ion laser as the excitation source.

2.3 Electrochemical measurements

All electrochemical experiments were performed using a CHI 730E electrochemical workstation or a WaveDrive10 potentiostat (Pine Instruments). Cyclic voltammetry (CV) measurements for ORR were conducted in a standard three-electrode cell using a glassy carbon (GC) electrode with the diameter of 3 mm as the working electrode, an Ag/AgCl (KCl, 3 M) electrode as reference electrode, and a Pt wire

as counter electrode. All obtained potentials *vs*. Ag/AgCl were converted to a reversible hydrogen electrode (RHE) scale using Nernst equation. A 0.10 M phosphate-buffered (PB) solution (pH 7.0) was used as the supporting electrolyte. Glassy carbon (GC) electrodes modified with the catalysts were fabricated by drop-coating 10 μL of the catalyst dispersion (2 mg/mL) onto the electrodes. Before the measurements, the electrolyte was bubbled with N_2 or O_2 for 20 min.

Rotating ring-disk electrode (RRDE) measurements were performed on WaveDrive10 potentiostat (Pine Instruments). For the electrode modification, 60 μL of the catalyst dispersion (2 mg/mL) was drop-coated onto GC disk electrodes (0.248 cm^2 in area) as working electrodes. A Pt wire was used as the counter electrode, and an Ag/AgCl (KCl, 3 M) electrode a Pt wire as the reference electrode. The working electrode was scanned cathodically at a rate of 10 $mV \cdot s^{-1}$ with the potential of the ring electrode set constantly at +0.50 V *vs*. Ag/AgCl (KCl, 3 M) electrode. Before the measurements, the electrolyte was bubbled with O_2 for 20 min. All the electrochemical measurements were performed at room temperature.

The electron transfer number (n) during ORR were calculated from the RRDE results on the basis of the following equations:

$$n = 4 \times \frac{I_D}{\frac{I_R}{N} + I_D}$$

where N is the collection efficiency calculated to be 0.37, I_D is the disk current, and I_R is the ring current from RRDE experiments.

The number of electrons involved in ORR can also be determined from RDE experiments according to Koutecky-Levich's equation:

$$\frac{1}{i} = \frac{1}{i_k} + \frac{1}{i_d} = \frac{1}{i_k} + \frac{1}{0.2nFACD^{2/3}v^{-1/6}\omega^{1/2}}$$

in which i_k, and i_d represent kinetic and diffusion-limiting current, respectively; F is Faraday constant (96485 $C \cdot mol^{-1}$); A is the geometric area of disk electrode (0.248 cm^2); C and D are the concentration (1.26×10^{-6} $mol \cdot cm^{-3}$) and diffusion coefficient (2.6×10^{-5} $cm^2 \cdot s^{-1}$) of O_2 in pH 7.0 phosphate-buffered solution, respectively; v is the kinetic viscosity of solution (0.009 $cm^2 \cdot s^{-1}$); ω is the rotation speed (rpm).

S2-Material characterizations and electrochemical measurements

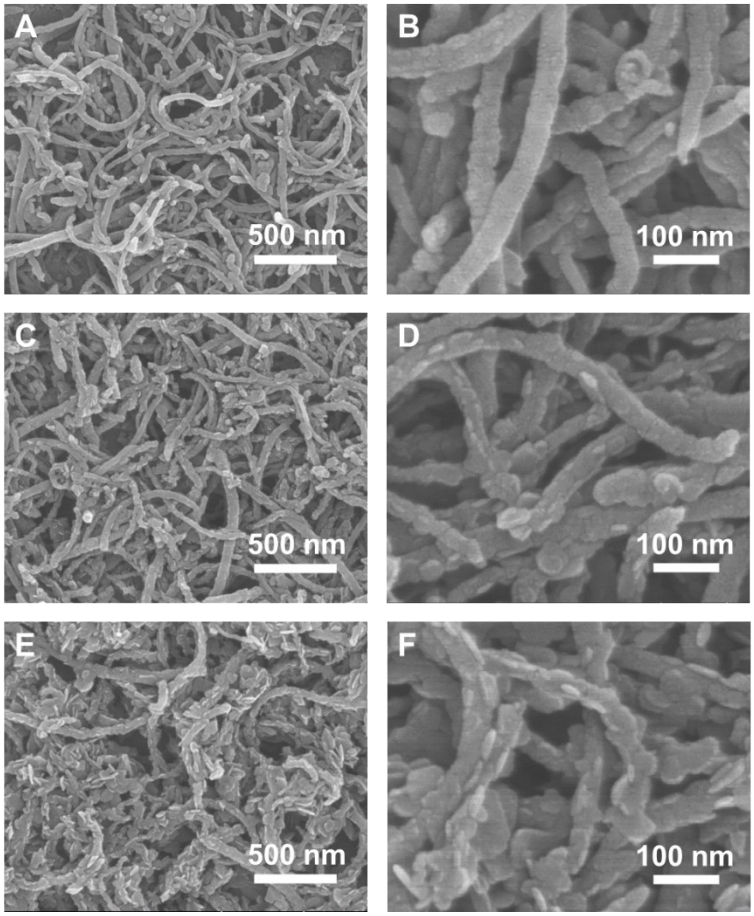

Fig. S1 SEM images of Co-MOF@CNT-**1** (A and B), Co-MOF@CNT-**2** (C and D), or Co-MOF@CNT-**3** (E and F).

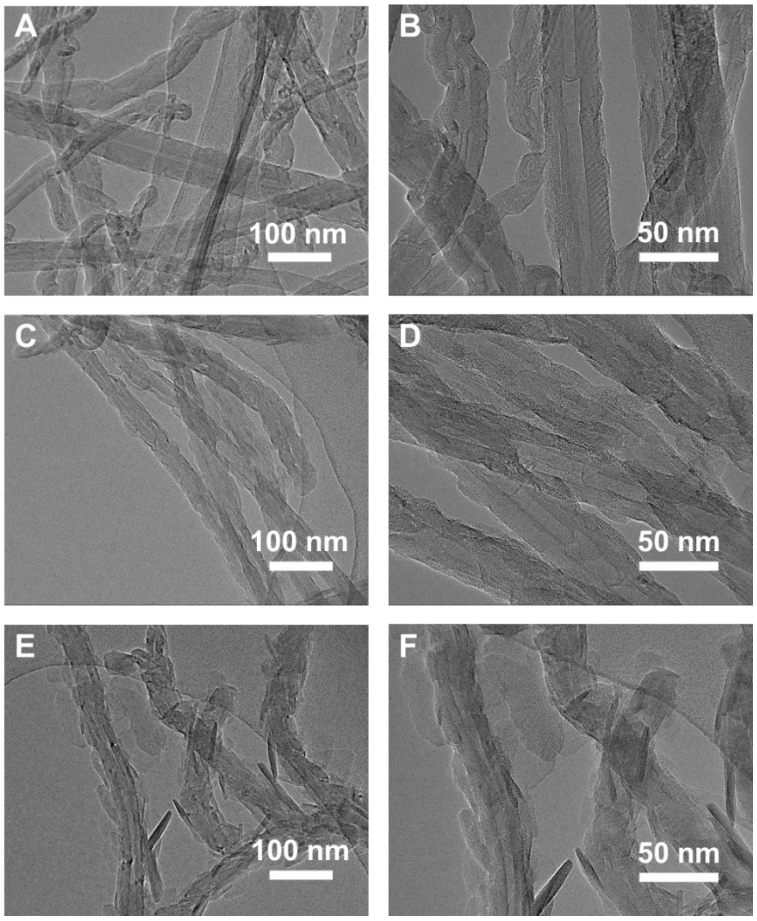

Fig. S2 TEM images of Co-MOF@CNT-**1** (A and B), Co-MOF@CNT-**2** (C and D), or Co-MOF@CNT-**3** (E and F).

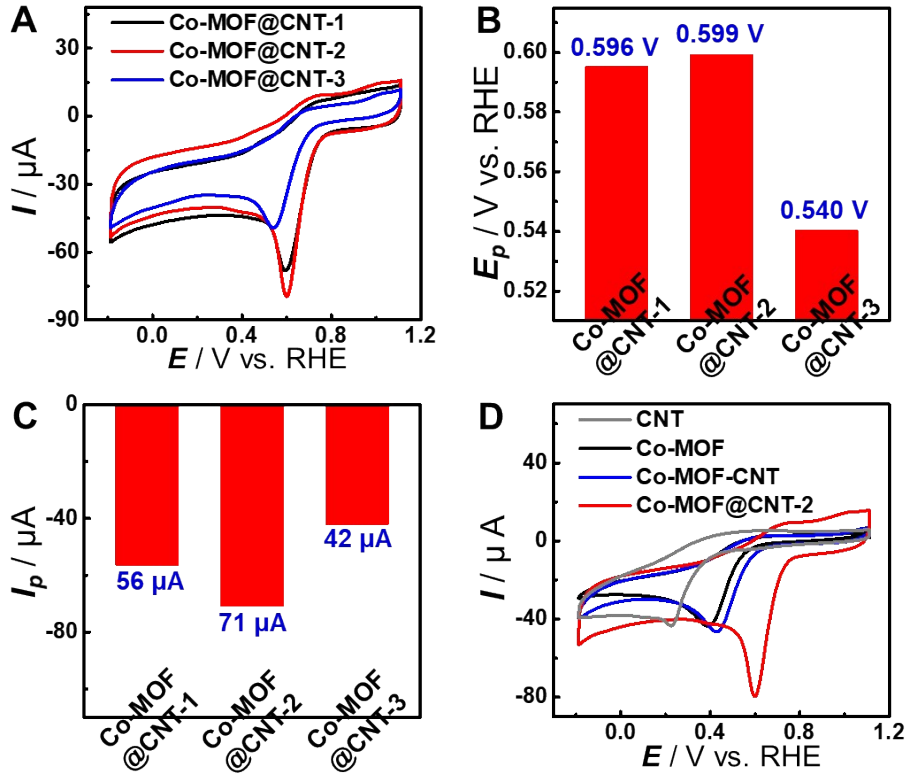

Fig. S3 (A) CV curves of GC electrodes modified with Co-MOF@CNT-**1** (black line), Co-MOF@CNT-**2** (red line), or Co-MOF@CNT-**3** (blue line) in O_2-saturated PB solution (pH 7.0). Potential scan rate, 50 mV·s^{-1}. (B-C) Histograms of the peak potentials (B) and peak currents (C) from CV curves of the catalysts. (D) CV curves of GC electrodes modified with CNT (grey line), Co-MOF (black line), Co-MOF-CNT (blue line), or Co-MOF@CNT-**2** (red line) in O_2-saturated PB solution (pH 7.0). Potential scan rate, 50 mV·s^{-1}.

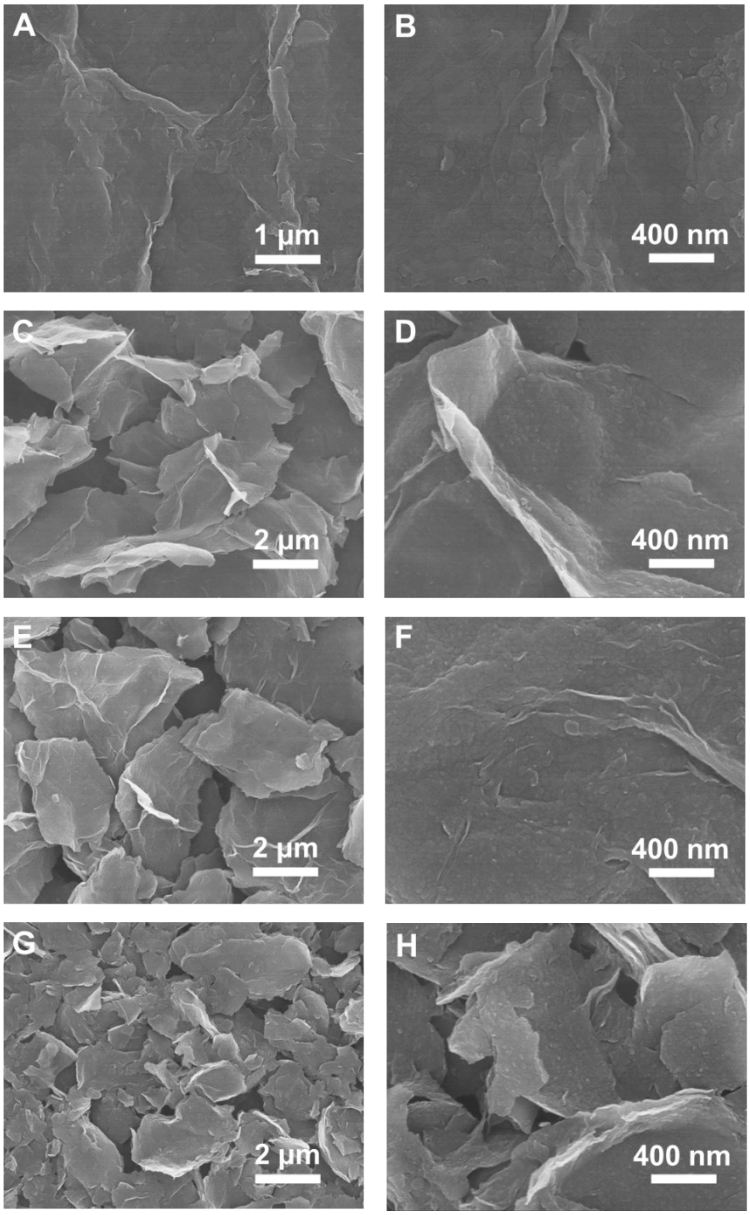

Fig. S4 SEM images of Co-MOF@rGO-**1** (A and B), Co-MOF@rGO-**2** (C and D), Co-MOF@rGO-**3** (E and F), or Co-MOF@rGO-**4** (G and H).

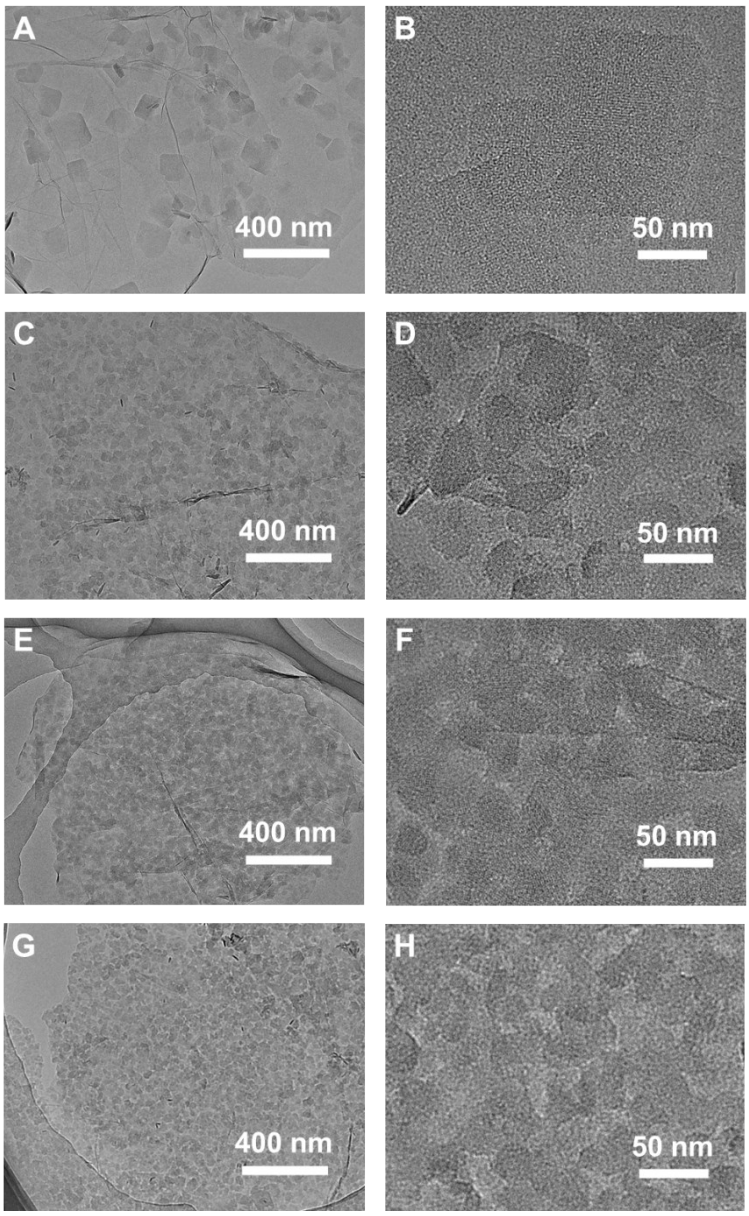

Fig. S5 TEM images of Co-MOF@rGO-**1** (A and B), Co-MOF@rGO-**2** (C and D), Co-MOF@rGO-**3** (E and F), or Co-MOF@rGO-**4** (G and H).

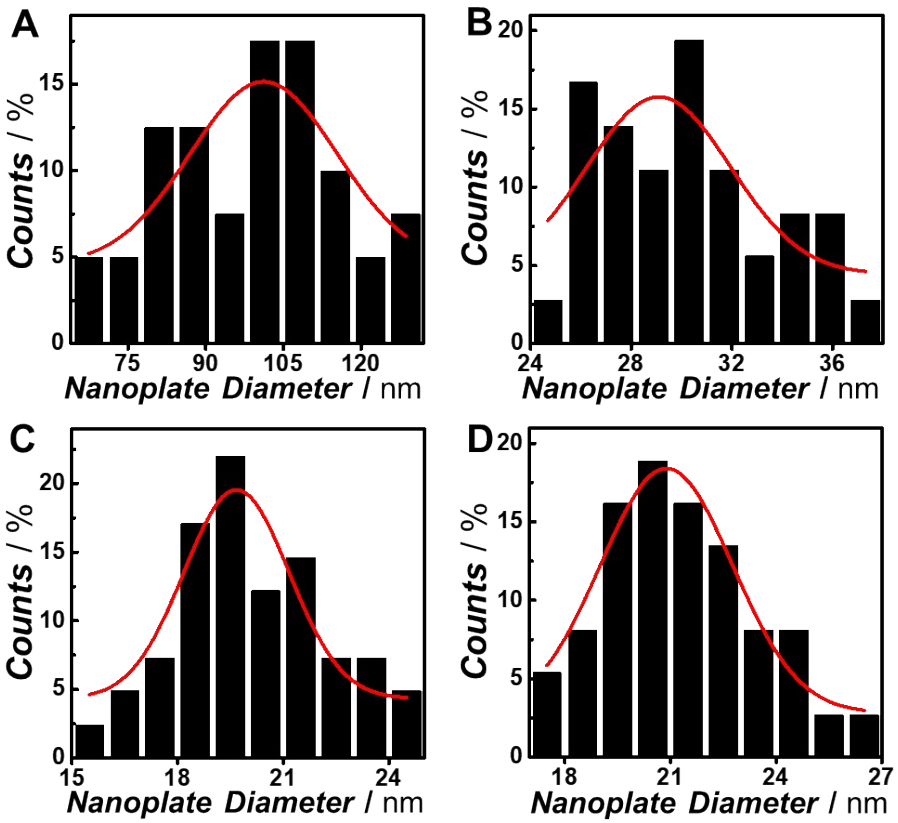

Fig. S6 The statistical size distribution analysis of Co-MOF nanoplates on Co-MOF@rGO-**1** (A), Co-MOF@rGO-**2** (B), Co-MOF@rGO-**3** (C), or Co-MOF@rGO-**4** (D).

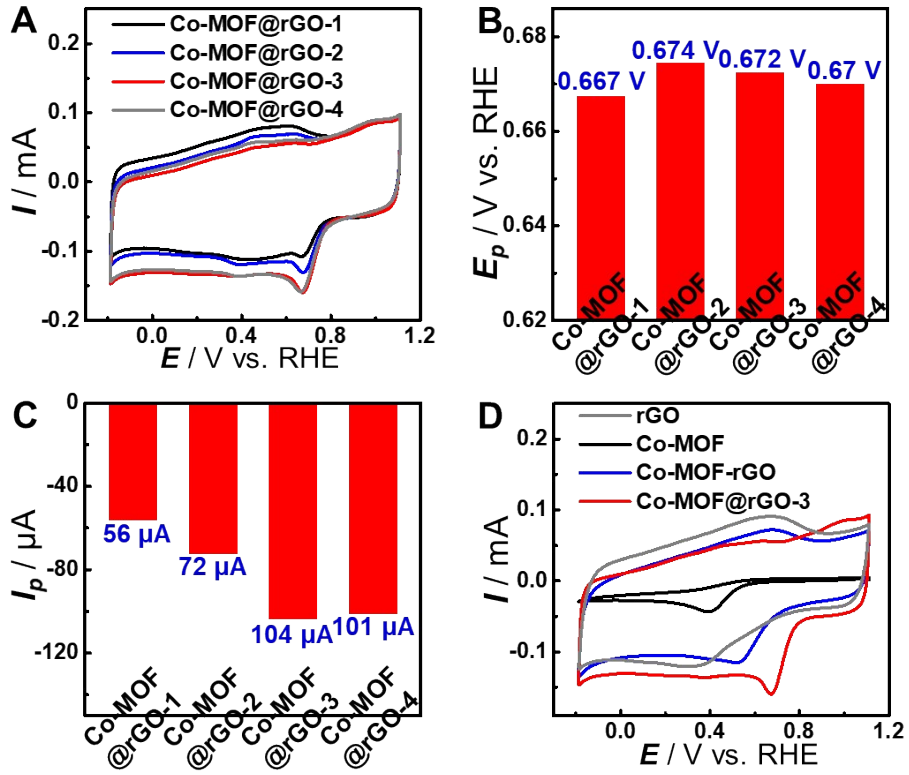

Fig. S7 (A) CV curves of GC electrodes modified with Co-MOF@rGO-**1** (black line), Co-MOF@rGO-**2** (blue line), Co-MOF@rGO-**3** (red line), or Co-MOF@rGO-**4** (grey line) in O_2-saturated PB solution (pH 7.0). Potential scan rate, 50 mV·s^{-1}. (B-C) Histograms of the peak potentials (B) and peak currents (C) from CV curves of the catalysts. (D) CV curves of GC electrodes modified with rGO (grey line), Co-MOF (black line), Co-MOF-rGO (blue line) and Co-MOF@rGO-**3** (red line) in O_2-saturated PB solution (pH 7.0). Potential scan rate, 50 mV·s^{-1}.

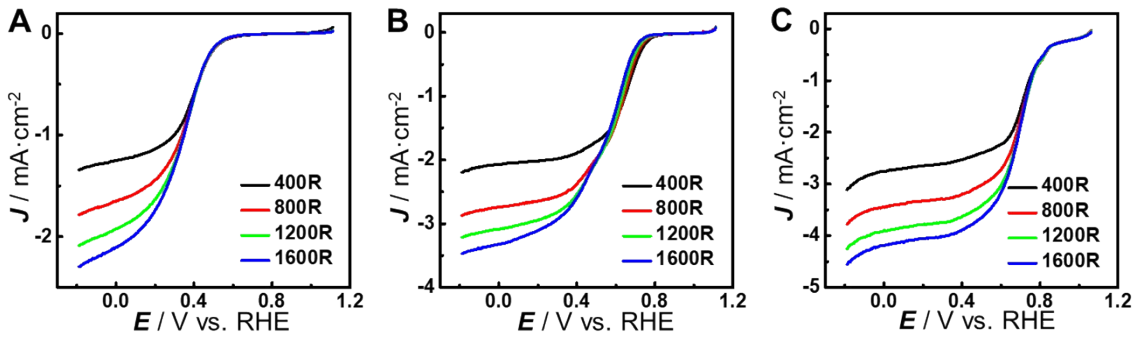

Fig. S8 Linear sweep voltammetry (LSV) curves of Co-MOF (A), Co-MOF@CNT-**2** (B), or Co-MOF@rGO-**3** (C) with various rotation rates in O_2-saturated PB solution (pH 7.0). Potential scan rate, 10 $mV \cdot s^{-1}$.

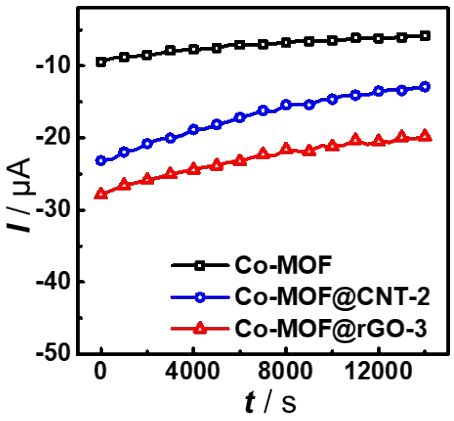

Fig. S9 Chronoamperometric responses obtained with Co-MOF (black square) at 0.39 V (vs. RHE), Co-MOF@CNT-**2** (blue circle) at 0.60 V (vs. RHE), or Co-MOF@rGO-**3** (red triangle) at 0.67 V (vs. RHE) in O_2-saturated PB solution (pH 7.0).

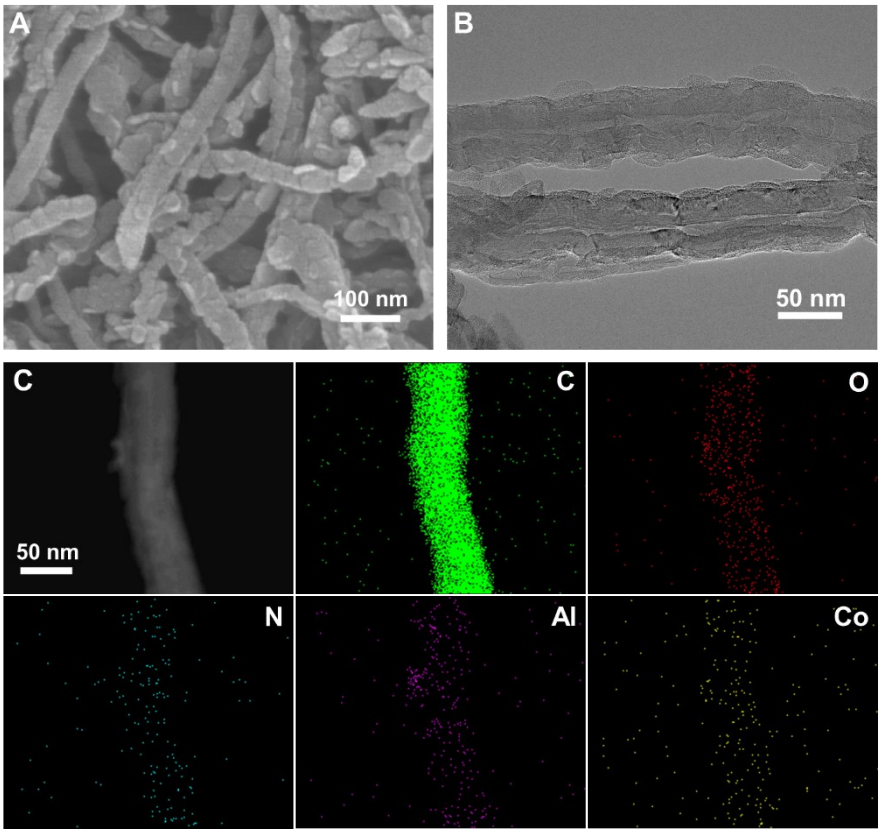

Fig. S10 SEM (A), TEM (B) images and corresponding C, O, N, Al and Co atom mapping (C) of Co-MOF@CNT-**2** after 4-h ORR test.

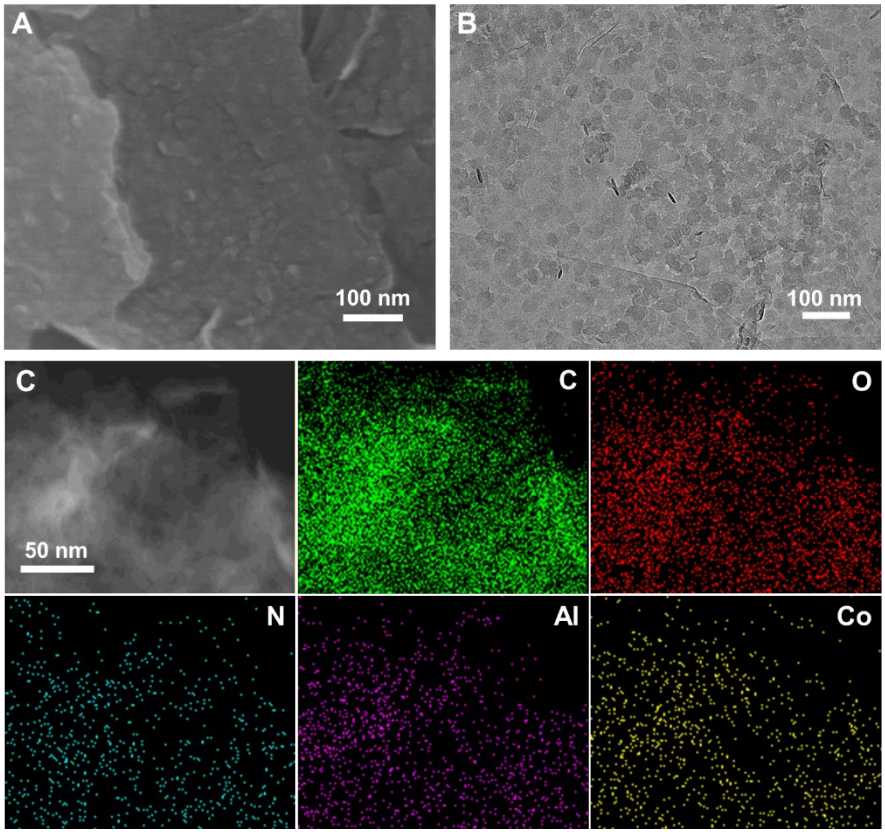

Fig. S11 SEM (A), TEM (B) images and corresponding C, O, N, Al and Co atom mapping (C) of Co-MOF@rGO-**3** after 4-h ORR test.

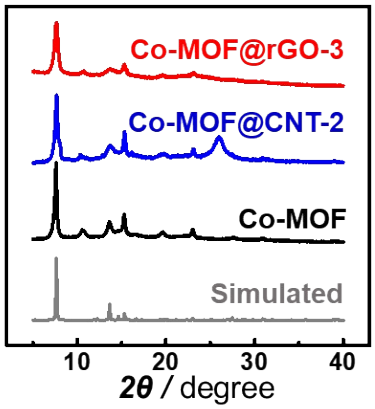

Fig. S12 PXRD patterns of simulated Co-MOF (light grey line), as-synthesized Co-MOF (black line), Co-MOF@CNT-**2** (blue line), or Co-MOF@rGO-**3** (red line).

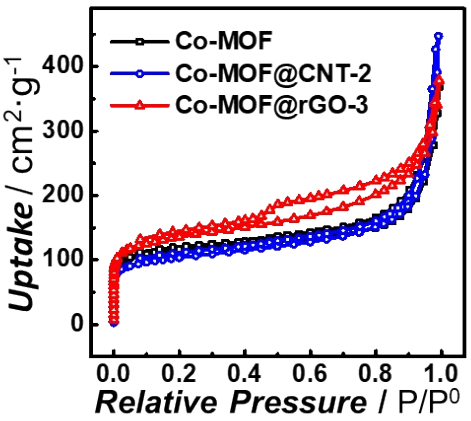

Fig. S13 Nitrogen sorption isotherms for Co-MOF (black square), Co-MOF@CNT-**2** (blue circle) and Co-MOF@rGO-**3** (red triangle).

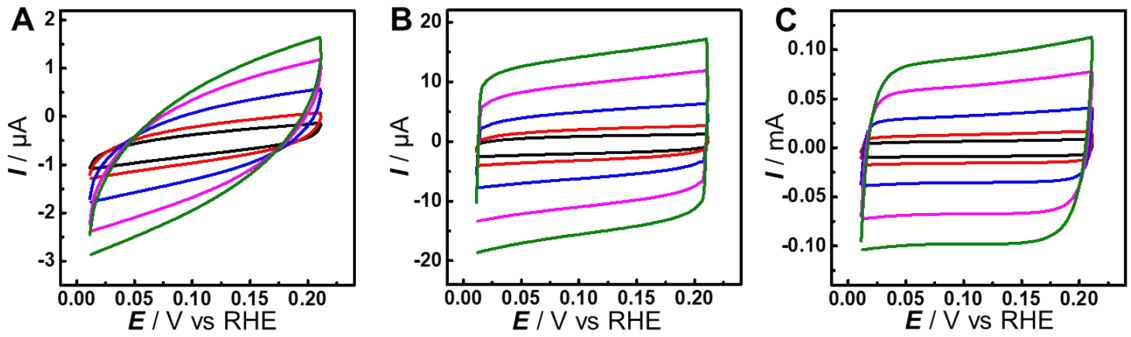

Fig. S14 CV curves of GC electrodes modified with Co-MOF (A), Co-MOF@CNT-**2** (B), or Co-MOF@rGO-**3** (C) at different scan rates ranging from 10 to 150 $mV \cdot s^{-1}$ in N_2-saturated PB solution (pH 7.0).

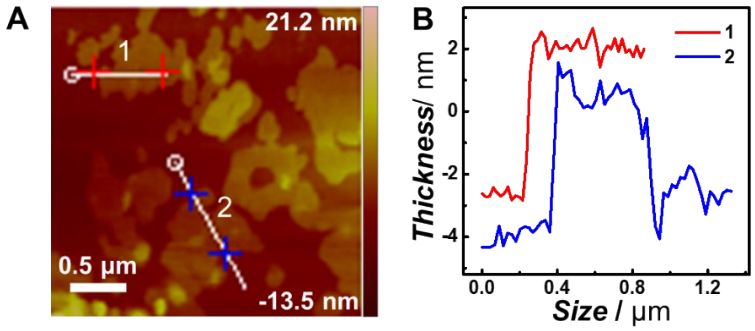

Fig. S15 (A) Atomic force microscope (AFM) image of Co-MOF@rGO-**3**. (B) The thickness of Co-MOF@rGO-**3** measured with AFM.

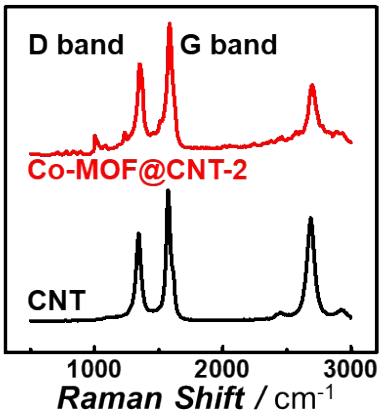

Fig. S16 Raman spectra of CNT (black line) and Co-MOF@CNT-**2** (red line).

S3-Density functional theory calculations

1 Methods

All the calculations was performed within the framework of the density functional theory (DFT) as implemented in the Vienna Ab initio Software Package (VASP 5.3.5) code within the Perdew–Burke–Ernzerhof (PBE) generalized gradient approximation and the projected augmented wave (PAW) method.[4-7] The cutoff energy for the plane-wave basis set was set to 450 eV. The Brillouin zone of the surface unit cell was sampled by Monkhorst–Pack (MP) grids, with k-point mesh for catalysts structure optimizations.[8] The convergence criterion for the electronic self-consistent iteration and force was set to 10^{-5} eV and 0.01 eV/Å, respectively. In this work, we set the Hubbard parameter to U − J = 4 for Co, which ensures a good qualitative description of structure and electronic properties of Co-based materials. A vacuum layer of 15 Å was introduced to avoid interactions between periodic images.

2 Calculations

The ORR through $2e^-$ and $4e^-$ pathways produces H_2O and H_2O_2, respectively. The $4e^-$ reaction includes several elementary steps:

$$* + O_2\,(g) + H^+ + e^- \rightarrow *OOH \qquad (a)$$

$$*OOH + H^+ + e^- \rightarrow *O + H_2O\,(l) \qquad (b)$$

$$*O + H^+ + e^- \rightarrow *OH \qquad (c)$$

$$*OH + H^+ + e^- \rightarrow H_2O\,(l) + * \qquad (d)$$

The $2e^-$ reaction is composed of several elementary steps:

$$* + O_2\,(g) + H^+ + e^- \rightarrow *OOH \qquad (e)$$

$$*OOH + H^+ + e^- \rightarrow H_2O\,(l) + * \qquad (f)$$

where the asterisk (*) denotes the active site of the catalyst.

The free energies of adsorbates at temperature T were estimated according to the harmonic approximation, and the entropy was evaluated using the following equation:

$$S(T) = K_B \sum_{i}^{harm\ DOF} \left(\frac{\varepsilon_i}{K_B T \left(e^{\frac{\varepsilon_i}{K_B T}} - 1 \right)} - ln\left(1 - e^{-\frac{\varepsilon_i}{K_B T}} \right) \right) \qquad (g)$$

where K_B is Boltzmann's constant and DOF is the number of harmonic energies (ε_i) used in the summation denoted as the degree of freedom, which is generally 3N, where N is the number of atoms in the adsorbates. Meanwhile, the free energies of gas phase species are corrected as:

$$G_g(T) = E_{elec} + E_{ZPE} + \int C_p dT - TS(T) \qquad (h)$$

where C_p is the gas phase heat capacity as a function of temperature derived from Shomate equations and the corresponding parameters in the equations were obtained from NIST.

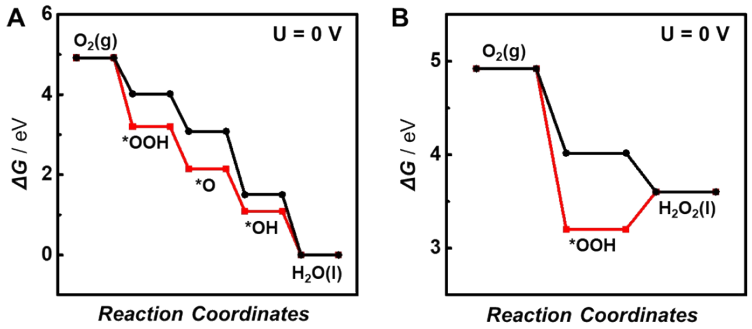

Fig. S17 Calculated reaction energetics on graphene- (red line) and CNT- (black line) supported Co-MOF models for $4e^-$ (a) and $2e^-$ (b) ORR at U = 0 V vs RHE.

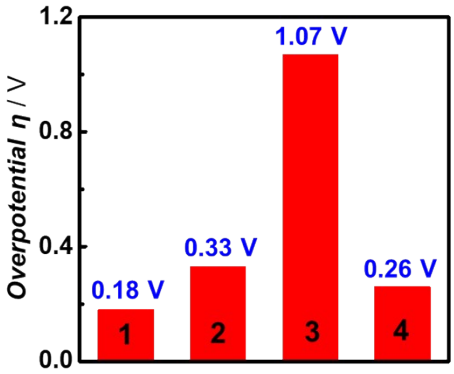

Fig. S18 The corresponding theoretical overpotentials (η) for $4e^-$ (1 and 2) and $2e^-$ (3 and 4) ORR at graphene- (1 and 3) and CNT- (2 and 4) supported Co-MOF models.

References

(1) Zhao, Y.; Kornienko, N.; Liu, Z.; Zhu, C.; Asahina, S.; Kuo, T.-R.; Bao, W.; Xie, C.; Hexemer, A.; Terasaki, O.; Yang, P.; Yaghi, O. M. Mesoscopic Constructs of Ordered and Oriented Metal–Organic Frameworks on Plasmonic Silver Nanocrystals. *J. Am. Chem. Soc.* **2015**, *137* (6), 2199-2202.

(2) Zhang, W.; Chi, Z.-X.; Mao, W.-X.; Lv, R.-W.; Cao, A.-M.; Wan, L.-J. One-Nanometer-Precision Control of Al_2O_3 Nanoshells through a Solution-Based Synthesis Route. *Angew. Chem. Int. Ed.* **2014**, *53* (47), 12776-12780.

(3) Huang, Z.; Zhou, A.; Wu, J.; Chen, Y.; Lan, X.; Bai, H.; Li, L. Bottom-Up Preparation of Ultrathin 2D Aluminum Oxide Nanosheets by Duplicating Graphene Oxide. *Adv. Mater.* **2016**, *28* (8), 1703-1708.

(4) Perdew, J. P.; Burke, K.; Ernzerhof, M., Generalized Gradient Approximation Made Simple. *Phys. Rev. Lett.* **1996,** *77* (18), 3865-3868.

(5) Hammer, B.; Hansen, L. B.; Nørskov, J. K. Improved adsorption energetics within density-functional theory using revised Perdew-Burke-Ernzerhof functionals. *Phys. Rev. B* **1999,** *59* (11), 7413-7421.

(6) Blöchl, P. E., Projector augmented-wave method. *Phys. Rev. B* **1994,** *50* (24), 17953-17979.

(7) Kresse, G.; Joubert, D. From ultrasoft pseudopotentials to the projector augmented-wave method. *Phys. Rev. B* **1999,** *59* (3), 1758-1775.

(8) Monkhorst, H. J.; Pack, J. D. Special points for Brillouin-zone integrations. *Phys. Rev. B* **1976,** *13* (12), 5188-5192.